Mass distributions in various nuclear collisions

S. J. Lee* and A. Z. Mekjian†
Department of Physics and Astronomy, Rutgers University, Piscataway, New Jersey 08855
(Received 18 September 1991)

The cluster size distributions in proton-nucleus collisions and in nucleus-nucleus collisions are discussed using a simple exactly soluble model. These distribution can be characterized by a single parameter involving volume, temperature, binding energy, and level density effects. As this parameter varies, the shape of the distribution of cluster size changes. Good agreement is found between a simple theoretical prediction and experiment.

PACS number(s): 24.60.−k, 25.40.Ve, 25.70.Mn

The main purpose of this paper is to illustrate an application of a recent model of a fragmentation process to some data on very-high-energy proton-nucleus and medium energy nucleus-nucleus collisions. Fragmentation phenomena induced by both protons and nuclei is of current interest and many reasons exist for looking at such collisions. Some of them are (1) to understand the underlying mechanisms, forces, and pathways that lead to the final distribution of products; (2) to produce nuclei at high temperature T and density ρ to see how nuclei behave as a function of T and ρ; (3) to search for phase transitions in the nuclear system; and, more recently, (4) to look for possible intermittent behavior in the distribution of products.

The fragmentation model initially developed in Ref. [1] and extended in Refs. [2–4] leads to a very simple expression for the distribution of fragments as a function of density and temperature. For example, the mean number of clusters $\langle n_k \rangle$ of size k is given by

$$\langle n_k \rangle = \left[\frac{x_k}{k} \right] \frac{A!}{(A-k)!} \frac{Q_{A-k}(\mathbf{x})}{Q_A(\mathbf{x})} . \tag{1}$$

Here $\mathbf{x}=(x_1,x_2,x_3,\ldots)$ and $Q_A(\mathbf{x})$ is the canonical partition function for a system with A particles which is given by

$$Q_A(\mathbf{x}) = \sum_{\{n_i\}_A} M_2(A,\mathbf{n}) \prod_i [x_i^{n_i}]$$

$$= \sum_{\{n_i\}_A} A! \prod_i \left[\frac{x_i^{n_i}}{i^{n_i} n_i!} \right] . \tag{2}$$

The sum in Eq. (2) is over all the possible combinations of n_i's with the constraint of

$$\sum_i i n_i = A . \tag{3}$$

The Cauchy's number $M_2(A,\mathbf{n}) = A!/\prod_i [i^{n_i} n_i!]$ contains the microstate counting rule for the partition $\mathbf{n}=\{n_i\}=(n_1,n_2,n_3,\ldots)$ and the x_i contains the thermodynamic weight for each cluster i. A normalized weight given to any partition $\mathbf{n}$ is $M_2(A,\mathbf{n}) \prod_i [x_i^{n_i}]/Q_A(\mathbf{x})$. In Ref. [4] the weighting parameter x_i is related to the thermodynamic partition function of a cluster of size i:

$$x_i(T) = x(v) \exp\left[-\int E_i(T) d(1/k_B T) \right]$$

$$= x(v) \exp\left[\int E_i(T) T^{-2} dT/k_B \right] . \tag{4}$$

When the x_i's are written in the form of Eq. (4), the exponential part is the path integral of the temperature-dependent Hamiltonian with the imaginary time T^{-1}. The $E_i(T)$ is the total energy at the temperature T of the cluster with i nucleons which is the sum of the thermal kinetic energy of the cluster and the internal energy of the cluster. The latter energy consists of the binding and excitation energies of nucleons in the cluster. The $x(v)$ represents the volume dependence of the partition function and k_B is the Boltzmann constant.

In Ref. [1] a particular choice $x_i = x$ was taken. More generally [4], if $x_i = x X_1^i$, then the canonical partition function of Eq. (2) is

$$Q_A(\mathbf{x}) = X_1^A Q_A(x) = X_1^A \frac{\Gamma(x+A)}{\Gamma(x)} , \tag{5}$$

and the mean number of clusters $\langle n_k \rangle$ of size k is given by

$$\langle n_k \rangle = \left[\begin{matrix} A \\ k \end{matrix} \right] x B(x+A-k,k)$$

$$= \left[\frac{x}{k} \right] \frac{A!}{(A-k)!} \frac{\Gamma(x+A-k)}{\Gamma(x+A)} . \tag{6}$$

The B is the beta function $B(a,b) = \Gamma(a)\Gamma(b)/\Gamma(a+b)$ and the Γ's are gamma functions. The $\left[\begin{matrix} A \\ k \end{matrix} \right] = A!/(A-k)!k!$ is the binomial factor. Here A is the total number of baryons in the system which may be partitioned among the clusters produced in the fragmentation process. Notice here that X_i disappears in $\langle n_k \rangle$ of Eq. (6): X_1 is the same for every nucleon independent of the cluster it belongs to. Thus X_1 in the $x_i = x X_1^i$ gives

*Electronic address: sjlee@ruthep.rutgers.edu.
†Electronic address: mekjian@ruthep.rutgers.edu.

the same weight X_1^A for every partition **n** in the canonical partition function $Q_A(\mathbf{x})$ of Eq. (2). The distribution $\langle n_k \rangle$ depends only on the variable x; thus we call this case with the x_i's in the form of xX_1^i the one-parameter x model. The x is a tuning parameter and this variable, which changes with temperature and density, contains the physical contents of the model. Note here that the weight x is independent of the cluster size and thus gives the same weight x^M for any partition **n** having the same multiplicity $M=\sum_i n_i$ [see Eq. (2)].

Once we know the thermal and internal energy of each cluster, thermodynamic arguments [1,3,4] establish the behavior of x_i through Eq. (4). If we neglect the surface tension and the Coulomb interaction, the total energy (binding, internal excitation, and translational) for a cluster of size i has the form of

$$E_i(T)=\tfrac{3}{2}k_BT+M_Bi-E_B(i)\ , \tag{7}$$

where the binding energy is given by

$$\begin{aligned} &E_B(i)=a_B(T)(i-f_i)\ , \\ &a_B(T)=a_B-\frac{1}{\epsilon_0}\left[\frac{k_BTT_0}{T+T_0}\right]^2 . \end{aligned} \tag{8}$$

The f_i can be taken in various ways which depend on how we account for the fact that the monomer has no internal structure. One way, considered in Ref. [4], takes $f_i=\delta_{i,1}$ and accounts explicitly for the fact that a free nucleon (monomer with $i=1$) has no internal or binding energy, $E_B(1)=0$. All the clusters with $i>1$ have the same binding energy per nucleon $E_B(i)/i=a_B(T)$. Then the thermodynamic partition function x_i becomes, according to Eq. (4),

$$\begin{aligned} &x_i=xy^{\delta_{i,1}}X_1^i\ ,\quad x=X_0\ , \\ &y=1/X_B\ ,\quad X_1=X_MX_B\ , \end{aligned} \tag{9}$$

where

$$\begin{aligned} X_0&\equiv x(v)\exp\left[\int\frac{(3/2)k_BT}{k_BT^2}dT\right] \\ &=\frac{V}{v_0}=V\frac{(2\pi M_Bk_BT)^{3/2}}{h^3}\ , \\ X_M&\equiv\exp\left[\int\frac{M_B}{k_BT^2}dT\right]=\exp\left[-\frac{M_B}{k_BT}\right]\ , \\ X_B&\equiv\exp\left[-\int\frac{a_B(T)}{k_BT^2}dT\right] \\ &=\exp\left[\frac{a_B}{k_BT}+\frac{1}{\epsilon_0}\frac{k_BTT_0}{(T+T_0)}\right] . \end{aligned} \tag{10}$$

The V and T are the freeze-out volume and temperature and are the thermodynamic variables associated with the fragmentation process. The v_0 is the quantum volume associated with the thermal de Broglie wavelength $\lambda_T^3=v_0$, where $\lambda_T=h/(2\pi M_Bk_BT)^{1/2}$. Planck's constant h appears because the fragmentation or break up of a cluster changes the number of clusters (particles) or multiplicity and each cluster has associated with it a volume in phase space $d^3r\,d^3p/h^3$. The a_B at $T=0$ is a coefficient in the binding-energy formulas for a cluster which is taken as $E_B(k)=a_Bk$. The ϵ_0 is the level spacing for excited states of a cluster while T_0 is a cutoff temperature introduced in Ref. [5] to limit the contribution of highly excited states to the internal partition function of a cluster.

For x_i's given by Eq. (9), the canonical partition function [4] becomes

$$\begin{aligned} Q_A(\mathbf{x})&=X_1^AQ_A(x,y) \\ &=X_1^A\sum_{r=0}^{A}\frac{A!}{r!(A-r)!}[x(y-1)]^{A-r}Q_r(x)\ . \end{aligned} \tag{11}$$

The mean number of clusters of size k is then given by Eq. (1) with this $Q_A(x,y)$. Similar to the case of Eq. (5), the distribution $\langle n_k \rangle$ is independent of X_1 and depends only on x and y; thus we call this case with the x_i's in the form of $xy^{\delta_{i,1}}X_1^i$ the two-parameter x-y model. The monomer is then treated differently from other clusters by taking $y\neq 1$ in this case. When $y=1$, Eq. (11) reduces to Eq. (5) and thus this x-y model becomes the x model with the distribution $\langle n_k \rangle$ given by Eq. (6).

In our studies of various limiting cases [2] and numerical comparisons showed that the x model and the x-y model with the same value of x, independent of the value of y, are quite similar to each other for small clusters except for the monomer, $1<k\lesssim A/3$. Equation (11) shows that the x-y model can also be approximated by the x model for $|x(y-1)|<1$. Thus we will use the x model for comparison with data in this paper.

Taking $y=1$, the x-y model reduces to the x model. The choice of $f_i=0$ in Eq. (8) gives $y=1$ with keeping the x and X_1 unchanged in Eq. (9);

$$x_i=xX_1^i\ ,\quad x=X_0\ ,\quad X_1=X_MX_B\ . \tag{12}$$

Equation (12) has the same thermal behavior (V and T dependences) as the x-y model of Eq. (9) for the same x value. However, the monomer here has a nonzero binding energy $E_B(1)=a_B$ which is unrealistic. Thus Eq. (12) should be considered only as an approximated version of the x-y model of Eq. (9).

As a more realistic binding energy, the x model of Ref. [1] uses a backshifted binding energy $E_B(k)=a_B(T)(k-1)$, i.e., $f_i=1$ in Eq. (8). Then the $E_B(i)$ has the property $E_B(i=1)=0$ so that monomers have no binding energy and also the binding energy per particle $E_B(i)/i$ saturate at a_B. Light clusters have a smaller binding energy per particle. In this case, the model becomes the one-parameter x model with

$$x_i=xX_1^i\ ,\quad x=X_0/X_B\ ,\quad X_1=X_MX_B\ . \tag{13}$$

The corresponding canonical partition function and the mean multiplicity distribution are given by Eqs. (5) and (6). In this x model with the backshifted binding energy, a monomer has the same weight x as any cluster.

As x increases from zero to infinity, the structure of

the solution Eq. (6) changes. With increasing x, the initial system breaks into more and more pieces. For very small x, the result of Eq. (6) gives Fermi result for the evaporation of a particle from a heated Fermi system [1]. A statistical evaporation approach to nuclear fragmentation is considered by Friedman and Lynch [6]. For large x, the solution is that of clusters embedded in a gas of nucleons where clusters are formed and destroyed by various collision processes with balanced forward and backward rates for the various processes. Specifically, the solution of Eq. (6) reduces to the Saha equation or law of mass action [1,3]. At $x=0$ ($T=0$), the A nucleons exist as a giant cluster while at $x\to\infty$, only individual nucleons exist as in a very hot system. At $x=1$, a hyperbolic power law results with $\langle n_k \rangle = 1/k$.

The x will be treated as a parameter and the high-energy proton-nucleus and nucleus-nucleus data will be analyzed using Eq. (6). Figures 1(a)–1(e) show how the

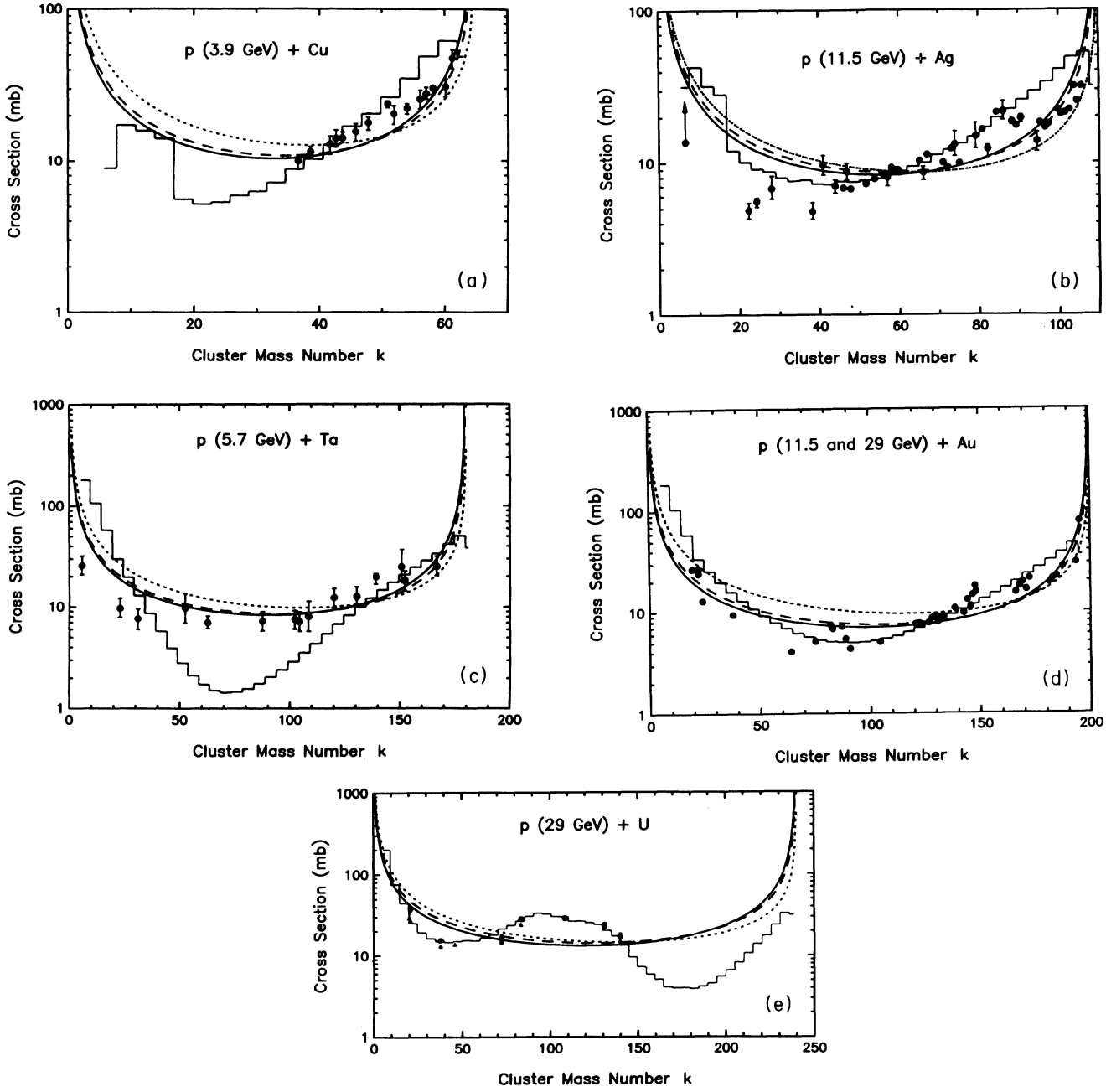

FIG. 1. (a) Fragment mass size distribution in the radiochemical measurements from the decay of a target residue produced in high-energy proton-nucleus collisions ($p+$Cu). The solid circles are the data summarized in Ref. [7] and the histograms are the thermodynamic statistical fits of Ref. [7]. The solid, dashed, and dotted lines are our model fits with $y=1$ and $x=0.3$, 0.1, and 0.01, respectively. Here $A=65$ is used in the fit. (b) Same as (a) but for $p+$Ag collisions. Here $A=110$ is used in the fit. (c) Same as (a) but for $p+$Ta collisions. Here $A=180$ is used in the fit. (d) Same as (a) but for $p+$Au collisions. Here $A=200$ is used in the fit. (e) Same as (a) but for $p+$U collisions. Here $A=240$ is used in the fit.

qualitative features of the proton-nucleus data can be understood in terms of Eq. (6). These figures are taken from the data summarized in Ref. [7] where these data and some statistical model calculations are compared. In particular, the histograms in Figs. 1(a)–1(e) are from this reference. As we can see, the simple x model of Eq. (6) fits the data with the same level of similarity as the thermodynamic statistical calculations of Ref. [7]. These cases show the U-shape distribution of cluster sizes and correspond to the case of small x, $x<0.3$. The small x indicates that the system breaks up at a low temperature [see Eqs. (12), (9), and (13) with Eq. (10) and Table I]. This is consistent with the fact that the data is taken through the radiochemical measurements which concerns the decay mode of the target residue after irradiation by a proton beam. Fragments produced directly from the proton-nucleus collision have escaped from the target residue system before the measurement. Only the delayed slow decay modes of the target residue, which is excited to a low-temperature thermal system, produces fragments which remain in the target system. Fragments produced in a hot system would have large enough kinetic energy to escape the target system before measurement.

In Table I we show X_0 which is the x in the x-y model Eq. (9) with the higher coexist density in a nuclear matter equation of state considered in Ref. [4]. Also shown are X_0/X_B which is the x in the x model of Eq. (13) with the higher spinodal density. With these choices of the density, the x model and the x-y model give similar values of temperature T for a same x value. Considering the fact that A ranges from ~ 65 to ~ 240, Table I shows that the temperature $k_B T$ corresponding to $x<0.3$ is less than 7 MeV. These temperature ranges are comparable to the temperature range $k_B T=4.4$ to 5.2 MeV in Ref. [7].

Similar fits as shown in Figs. 1(b) and 1(d) have been given in Ref. [8] with $x=0.01$. However the data of Fig. 1(b) in Ref. [8] comes from two completely different methods of extractions in the 300-GeV proton on the Ag target; the low mass part comes from an interpolation of a $p+\mathrm{Kr}$ collision [shown in Fig. 2(a)] and a $p+\mathrm{Xe}$ collision. The latter is obtained through a direct counter measurement in the $p+\mathrm{Xe}$ collision [10]. The large mass part comes from the radiochemical measurement. The large mass region (radiochemical measurement) corresponds to a break up of a low-temperature thermal system. On the other hand, the small mass region (counter-measurement) corresponds to a break up of a hot thermal system having a large $x>1$. Unless $x/A \ll 1$, $\langle n_k \rangle$ decreases exponentially as the cluster size k increases for the $k \ll A$ region [see Eq. (15) below]. This suggests that the $p+\mathrm{Ag}$ data considered in Ref. [8] should be fitted with two different values of x, a large x [cf., $x \approx 0.1A \approx 10$ for Fig. 2(a)] for the small mass fragmentation region and a small x [$x<0.3$ as in Fig. 1(b)] for the large mass region. The shoulder which appears at k near A cannot be accounted for in the simple x model. Reference [8] suggests using a k dependent x_k. We will look at this shoulder in a future paper.

The quantity x/A is an intensive quantity where the V in x [see X_0 of Eq. (10)] and the A result in $1/\rho = V/A$. For clusters of $k \ll A$ with large A which can have a large n_k, the solution $\langle n_k \rangle / A$ of Eq. (6) can be approximated [2] by

$$\frac{\langle n_k \rangle}{A} \approx \frac{1}{k}\left[\frac{x_k}{A}\right] e^{-\lambda k}, \tag{14}$$

TABLE I. Temperature dependence of the parameter x. The free volume factor is taken to be $V=(A/\rho_0)(\rho_0/\rho-1)$. The ρ_0 is the nuclear matter saturation density and ρ is the higher nuclear density of the coexist or spinodal point at the corresponding T for a nuclear matter equation of state considered in Ref. [4]. See Eqs. (9)–(13) for the various relations of X_0, X_B, x, and y.

		Coexist		Spinodal	
$k_B T$ (MeV)	$y=1/X_B$	ρ/ρ_0	X_0/A	ρ/ρ_0	X_0/AX_B
1.00	0.000 000 13	0.999 24	0.000 004 98	0.676 91	0.000 000 04
2.00	0.000 336 29	0.995 70	0.000 079 98	0.676 14	0.000 002 98
3.00	0.004 442 7	0.989 67	0.000 355 19	0.674 77	0.000 072 86
4.00	0.015 846	0.981 44	0.000 990 50	0.672 62	0.000 404 03
5.00	0.033 550	0.970 94	0.002 191 4	0.669 54	0.001 212 3
6.00	0.054 807	0.958 30	0.004 188 2	0.665 44	0.002 651 8
7.00	0.077 283	0.943 66	0.007 240 6	0.660 31	0.004 821 6
8.00	0.099 479	0.927 13	0.011 646	0.654 17	0.007 792 4
9.00	0.120 57	0.908 79	0.017 744	0.647 02	0.011 629
10.00	0.140 15	0.888 70	0.025 933	0.638 90	0.016 402
11.00	0.158 10	0.866 85	0.036 696	0.629 80	0.022 201
12.00	0.174 42	0.843 19	0.050 621	0.619 67	0.029 140
13.00	0.189 20	0.817 64	0.068 456	0.608 45	0.037 369
14.00	0.202 56	0.789 95	0.091 209	0.596 05	0.047 089
15.00	0.214 63	0.759 84	0.120 24	0.582 27	0.058 578
16.00	0.225 54	0.726 84	0.157 50	0.566 86	0.072 225
17.00	0.235 41	0.690 19	0.206 02	0.549 36	0.088 632
18.00	0.244 36	0.648 55	0.270 98	0.529 06	0.108 77
19.00	0.252 47	0.599 32	0.362 56	0.504 42	0.134 52
20.00	0.259 86	0.535 54	0.507 95	0.471 48	0.170 60

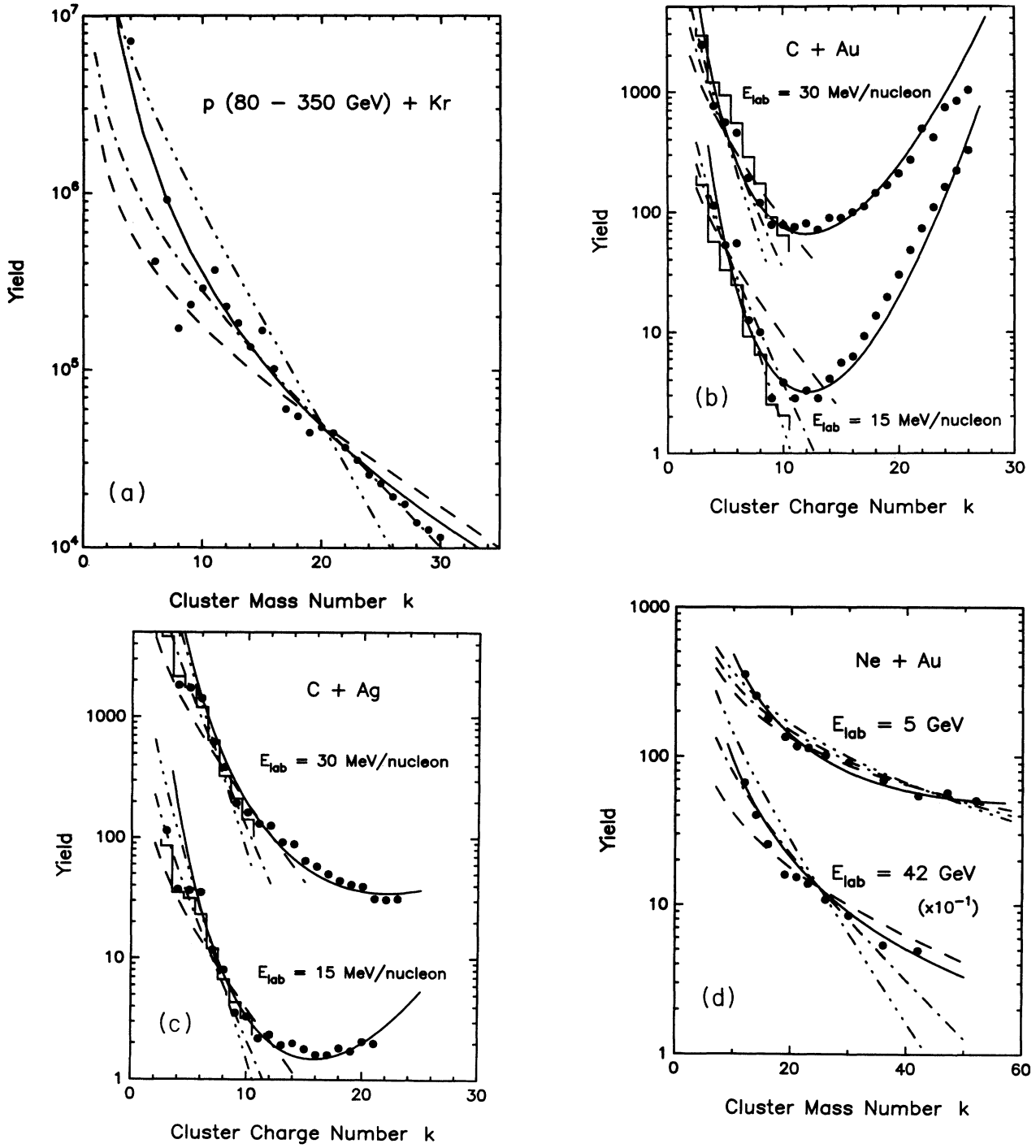

FIG. 2. (a) The cluster-size distribution resulting from a p + Kr reaction. The proton beam energies are 80–350 GeV. The data (solid circles) and the solid line are from Ref. [9]. Our model fits for $y=1$ are the dashed, dash-dotted, and dash-dot-dot-dotted curves with $x/A=0.06$, 0.1, and 0.2, respectively, and $A=80$. (b) The cluster charge distribution resulting from a C+Au reaction. The data (solid circles) and the solid line are from Ref. [9]. Our model fits for $y=1$ are the dashed, dash-dotted, and dash-dot-dot-dotted curves with $x/A=0.1$, 0.2, and 0.3, respectively, and $A=200$. Here the mass number A is considered to be twice the charge number Z in our comparison with data. Histograms are the fit of Ref. [12] using the statistical emission model of Ref. [6]. (c) The cluster charge distribution resulting from a C+Ag reaction. The data (solid circles) and the solid line are from Ref. [9]. Our model fits for $y=1$ are the dashed, dash-dotted, and dash-dot-dot-dotted curves with $x/A=0.1$, 0.2, and 0.3, respectively, and $A=120$. Here the mass number A is considered to be twice the charge number Z in comparison with data. Histograms are the fit of Ref. [12] using the statistical emission model of Ref. [6]. (d) The cluster-size distribution resulting from a Ne+Au reaction. The data (solid circles) and the solid line are from Ref. [9]. Our model fits for $y=1$ are the dashed, dash-dotted, and dash-dot-dot-dotted curves with $x/A=0.006$, 0.01, and 0.014, respectively, for the beam energy of 5 GeV, and with $x/A=0.02$, 0.06, and 0.1, respectively, for the beam energy of 42 GeV. Here $A=200$ has been used.

where the Lagrange multiplier λ is determined through the constraint of Eq. (3). For the case of $\lambda > 0$ and large A, Eq. (14) reduces to

$$\frac{\langle n_k \rangle}{A} \approx \frac{1}{k} \left[\frac{x}{A} \right] \left[\frac{1}{1+x/A} \right]^k , \tag{15}$$

in the x model. The distribution $\langle n_k \rangle / A$ is independent of the system size A when the intensive quantity x/A is held fixed and is further simplified to $\langle n_k \rangle / A \approx (1/k)(A/x)^{k-1}$ as $\lambda \to \infty$, i.e., $x \to \infty$.

Another set of data we have considered are those given and analyzed in Ref. [9]. These data are shown in Figs 2(a)–2(d). Also considered here are the data quoted in Ref. [11] which are shown in Fig. 3. In contrast to the case of Fig. 1, the data of Figs. 2 and 3 are obtained from a more direct measurement of the collision events. Thus the fragments measured are the fragments produced which then have escaped from the target system to the detector system instead of staying in the target system. The fragments are either fast or slow depending on the measurement details. These cases considered in Figs. 2 and 3 show larger values of $x\,(x > 1)$ corresponding to higher beam energies. Thus the system reaches a higher temperature before its break up. Since these data show only small clusters ($k \ll A$), we use the intensive quantity x/A appearing in Eq. (15) when analyzing the data.

Figure 2(a) shows the fragment distribution from p + Kr reaction with a gas-jet target [10]. The kinetic energy of the fragment ranges from 5 to 100 MeV. The fragments in these data are produced through the fragmentation of a highly excited nuclear remnant which has had sufficient time for many random nucleon-nucleon collisions [10]. The fit shown in Fig. 2(a) is obtained in our model with $x/A \approx 0.1$. This value corresponds to the temperature of $k_B T \approx 18$ MeV in the x model ($x = X_0/X_B$ with the spinodal density in Table I) and to $k_B T \approx 14$ MeV in the x-y model ($x = X_0$ with the coexist density). This is comparable to the temperature of 14 MeV used in Ref. [9].

Figures 2(b) and 2(c) show the fragment charge distributions instead of mass distributions. In the fit given here we have used $A = 2Z$. Also shown by the histograms are the fit of Ref. [12] using the statistical emission model of Ref. [6]. These data show a rise in the mass distribution for larger clusters due to a fission tail which cannot be considered in our simple model. To account for the fission peak we need to use a k dependent x_k. This k dependence may be related to a more complicated size dependence of the binding energy than Eq. (8) and destroy the exact solubility of the model. Thus we considered here only the small cluster region. However, the angular dependence of these data [12] indicates that the emission time scale is smaller than the time scale for reaching global equilibrium. Thus small clusters measured would be produced in a fragmentation process of a smaller thermal system than the whole nucleus (the number of participants is smaller than A) with higher temperature. These figures show that the lower energy (15 MeV/nucleon) reaction has larger x/A values compared to higher-energy reaction. However, larger x/A values

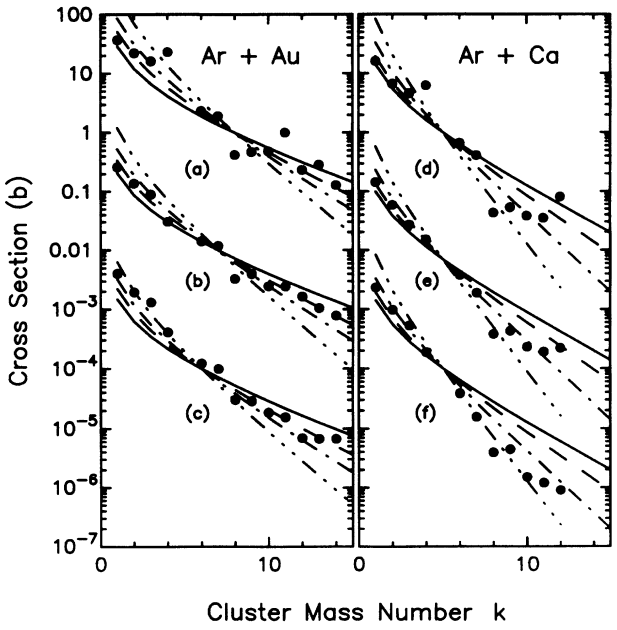

FIG. 3. The cluster-size distribution resulting from Ar+Au and Ar+Ca reactions. The data (solid circles) are taken from Ref. [11]. The beam energies are 42 MeV/nucleon for (a) and (d), 92 MeV/nucleon for (b) and (e), and 137 MeV/nucleon for (c) and (f). The cross sections in the figures are reduced by $\times 10^{-2}$ for (b) and (e) and by $\times 10^{-4}$ for (c) and (f). Our model fits for $y = 1$ are the solid, dashed, dash-dotted, and dash-dot-dot-dotted curves with $x/A = 0.2$, 0.3, 0.4, and 0.6, respectively, and $A = 240$ for Ar+Au reaction, and with $x/A = 0.3$, 0.4, 0.6, and 1.0, respectively, and $A = 80$ for Ar+Ca reaction.

do not necessarily mean higher temperatures. Larger x/A values can also occur from a smaller number of participants A for fixed x or from a larger x due to the larger freeze out volume V [see Eq. (10)]. In a low-energy collision, mean-field effects also become important along with the random nucleon-nucleon collisions which are required to form thermalized participants. For these reactions, Table I shows that the corresponding temperature is about 20 MeV in the x model and about 17 MeV in the x-y model. In the fits shown in Figs. 2(b) and 2(c), the number of participants used are $A = 200$ for C+Au reaction and $A = 120$ for C+Ag reaction. We would expect a much lower temperature in these low-energy reactions. To extract a correct temperature, we need to know the correct freeze-out volume and effective size A.

Figure 2(d) shows the distribution of slow fragments produced in Ne+Au reaction. In each collision event, fast fragments would be emitted through the direct breaking up due to the collision or through the decay of a local hot spot. On the other hand, the slow fragments would be emitted through the decay modes of a rather globally equilibrated hot thermal system. These fits show that the corresponding x/A values are ~ 0.01 for $E_{\rm lab} = 5$ GeV and 0.06 for $E_{\rm lab} = 42$ GeV reaction. The corresponding temperatures are about 9 and 15 MeV, respectively, for $E_{\rm lab} = 5$ and 42 GeV reactions if we use $x = X_0/X_B$ with the spinodal density. If we use $x = X_0$

with the coexisting density, then the corresponding temperatures are about 8 and 13 MeV. In Ref. [9] the temperature of 16 MeV has been used in the fit for the data of both energy. This $k_B T = 16$ MeV is comparable with our values for the $E_{\text{lab}} = 42$ GeV data. These data show that the higher energy reaction produces a hotter fireball than the lower energy reaction.

Figure 3 shows the energy and target dependences of the fragment distribution. The fragments here are produced from the decay of a thermalized subset of the target and projectile nucleons which formed a fireball. Table I shows that the corresponding temperature is more than about 20 MeV in the x model and more than about 17 MeV in the x-y model. The larger value of x corresponds to the higher temperature of the fireball. These figures show that the higher energy reaction produces a hotter fireball before its decay into fragments than the lower energy reaction. They also show that the smaller target system achieves a higher temperature before its break up than a larger target for the same beam energy. There are more participant nucleons to share the beam energy in forming a fireball in a larger target system than in a smaller target system.

In conclusion, a simple exactly soluble model was able to describe the overall behavior of nuclear fragmentation process in a wide range of reactions. The model gives a simple result for the distribution of cluster sizes in terms of a single parameter. This parameter contains a combination of quantities that govern the fragmentation process such as volume and temperature effects and binding energy and level density parameters. As the parameter varies from small to large values, the distribution of cluster sizes changes its shape from a U-shaped behavior to an exponential fall off with cluster size k. Temperatures extracted with this simple model for various data are similar to the values obtained with other models [6,7,9]. However, there is some uncertainty in determining the temperature in the simple model due to the unknown values of the break-up volume V and the effective size of the participants A.

This work was supported by National Science Foundation Grant No. 89-03457. We would like to thank L. Zamick for an interesting discussion.

[1] A. Z. Mekjian, Phys. Rev. C **41**, 2103 (1990); Phys. Rev. Lett. **64**, 2125 (1990).
[2] S. J. Lee and A. Z. Mekjian, Phys. Lett. A **149**, 7 (1990).
[3] A. Z. Makjian and S. J. Lee, Phys. Rev. A **44**, 6294 (1991).
[4] S. J. Lee and A. Z. Mekjian, Phys. Rev. C (to be published).
[5] S. Koonin and J. Randrup, Nucl. Phys. **A474**, 173 (1987).
[6] W. A. Friedman and W. G. Lynch, Phys. Rev. C **28**, 16 (1983).
[7] D. H. E. Gross, L. Satpathy, M. Ta-chung, and M. Satpathy, Z. Phys. A **309**, 41 (1982). For the details of experiment, see the references in this one.
[8] P. J. Karol and K. L. Kolsky, Phys. Rev. C **43**, 908 (1991).
[9] A. L. Goodman, J. I. Kapusta, and A. Z. Mekjian, Phys. Rev. C **30**, 851 (1984). See the references therein for the details of experiment.
[10] J. F. Finn *et al.*, Phys. Rev. Lett. **49**, 1321 (1982); A. S. Hirsch *et al.*, Phys. Rev. C **29**, 508 (1984).
[11] B. V. Jacak *et al.*, Phys. Rev. C **35**, 1751 (1987).
[12] C. B. Chitwood *et al.*, Phys. Lett. **131B**, 289 (1983).